Non-Gaussian Turbulence Induced Buffeting Responses of Long-Span Bridges

Wei Cui, A.M.ASCE[1]; Lin Zhao[2]; and Yaojun Ge[3]

Abstract: Conventionally, for turbulence-induced buffeting vibrations, the Gaussianity assumption is applied to all three subsequent stages of turbulence, wind loads, and structural vibrations because of its wide applicability and mathematical simplicity. However, non-Gaussian turbulence does exist in the boundary-layer atmosphere, especially near the tropical cyclone center. Non-Gaussian turbulence represents short duration and high-speed airflow, which is unfavorable for structural dynamic performance and reliability. It is necessary to analyze the non-Gaussian turbulence effect on flexible structures, especially long-span bridges, and compare the wind-induced vibration against responses caused by conventional Gaussian turbulence. The time domain bridge buffeting analysis method with unsteady aeroelastic force and aerodynamic admittance approximated by rational function was employed to calculate the vibrations excited by Gaussian and non-Gaussian turbulence, which were simulated using the spectrum representation method and the Hermit polynomial translation process method. A Monte Carlo simulation of bridge buffeting was conducted in this study. The statistical results show that the bridge response, excited either by Gaussian or non-Gaussian turbulence, still follows the Gaussian process assumption. However, for the same wind speed, Monte Carlo simulation shows that the vibration amplitudes increases with turbulence skewness in terms of RMS and extreme values. However, the increment ratio decreases with greater mean wind speeds. The peak factors also increase slightly for greater turbulence skewness. **DOI: 10.1061/(ASCE)BE.1943-5592.0001747**.

Author keywords: Bridge buffeting; Time domain analysis; Non-Gaussian turbulence; RMS response; Extreme response.

Introduction

The wind turbulence-induced structural buffeting response is a decades-old research field for flexible structures, such as long-span bridges and tall buildings. In the beginning stages, the foundation of the wind engineering analysis procedure was established in Alan Davenport's Ph.D. dissertation (Davenport 1961). The wind-induced structural response can be determined in both the frequency domain and the time domain through a combination of wind climatology, structural aerodynamics, and structural dynamic properties. Currently, this approach is designated as the *Davenport chain* (Isyumov 2012).

Initially, Davenport brought the statistical concept into the structural buffeting calculation procedure through random vibration theory (Davenport 1962). This became the fundamental theory in the frequency domain buffeting analysis framework. To improve the buffeting force accuracy, the frequency-dependent aerodynamic admittance function was introduced to transfer the wind turbulence spectrum to the aerodynamic force spectrum. For line-like structures, such as long-span bridges, the joint acceptance function is also needed to calculate the turbulence correlation decay function, depending on frequency, wind speeds, and three-dimensional spatial distance. This theory was also used for considering buffeting responses in tall buildings (Piccardo and Solari 1998, 2000) and wind directionality in vertical structures (Cui and Caracoglia 2017, 2018).

Next, the bridge section aeroelasticity was found to be critical to the bridge buffeting response (Scanlan and Jones 1990), because aerodamping and aerostiffness caused by motion-dependent aeroelasticity dramatically change the structural dynamic behavior. It was suggested that the turbulence-induced aerodynamic force and motion-induced aeroelastic force should be analyzed simultaneously. Meanwhile, long-span bridges are a special type of structure with closely spaced modal frequencies; thus, multimode coupling effects must be considered for wind-induced bridge buffeting. Jain et al. (1996) proposed an elegant formulation based on dimensionless time and frequency to study the multimode coupling effect on bridge buffeting and fluttering response. For super-long-span bridges with varying section shapes, location-dependent aeroelasticity properties can also be included in this method, which was applied to the Akashi Kaikyo Bridge in Japan (Katsuchi et al. 1999).

As computational power increased in recent decades, the time domain bridge buffeting method became another popular alternative approach, and is now a powerful tool for the multisource nonlinearity analysis (geometry, material, and aeroelasticity) of bridge wind-induced vibration. The indicial function from aerospace engineering was implemented to calculate the time-varying aeroelastic forces on the bridge deck (Scanlan 1984). Based on the quasi-stationary

[1]Assistant Professor, State Key Laboratory of Disaster Reduction in Civil Engineering, Tongji Univ., Shanghai 200092, China; Key Laboratory of Transport Industry of Wind Resistant Technology for Bridge Structures (Tongji Univ.), Shanghai 200092, China; Dept. of Bridge Engineering, College of Civil Engineering, Tongji Univ., Shanghai 200092, China. ORCID: https://orcid.org/0000-0001-7489-923X. Email: cuiwei@tongji.edu.cn

[2]Professor, State Key Laboratory of Disaster Reduction in Civil Engineering, Tongji Univ., Shanghai 200092, China; Key Laboratory of Transport Industry of Wind Resistant Technology for Bridge Structures (Tongji Univ.), Shanghai 200092, China; Dept. of Bridge Engineering, College of Civil Engineering, Tongji Univ., Shanghai 200092, China (corresponding author). Email: zhaolin@tongji.edu.cn

[3]Professor, State Key Laboratory of Disaster Reduction in Civil Engineering, Tongji Univ., Shanghai 200092, China; Key Laboratory of Transport Industry of Wind Resistant Technology for Bridge Structures (Tongji Univ.), Shanghai 200092, China; Dept. of Bridge Engineering, College of Civil Engineering, Tongji Univ., Shanghai 200092, China. Email: yaojunge@tongji.edu.cn

Note. This manuscript was submitted on July 1, 2020; approved on March 26, 2021; published online on June 10, 2021. Discussion period open until November 10, 2021; separate discussions must be submitted for individual papers. This paper is part of the ***Journal of Bridge Engineering***, © ASCE, ISSN 1084-0702.

concept, Roger's rational function aeroelastic force approximations were used to express the unsteady aerodynamic force.

The major challenge for time domain analysis is the number of frequency-dependent variables, such as the aeroelastic derivatives, bridge section admittance function, and turbulence spatial coherence. To overcome this difficulty, Chen et al. (2000a, 2000b) proposed to use the rational function with frequency-independent coefficients to approximate frequency-dependent factors. This method has been widely used for bridge buffeting analysis in recent decades. Many further studies were developed, aimed at aeroelastic nonlinearity (Diana et al. 2010; Wu and Kareem 2013; Yang et al. 2015), wind–vehicle–bridge coupled systems (Xu and Guo 2003; Cai and Chen 2004), transient wind response (Le and Caracoglia 2015, 2019), and stress level buffeting analysis (Xu et al. 2019). In recent years, in light of the nonstationarity of strong wind events (Wang et al. 2016), such as downbursts and tornados, time domain methods have become powerful tools for modeling nonstationary aeroelastic and aerodynamic (Hu et al. 2017) forces, for studying the interaction between fluid and rigid bodies.

The original method of Chen et al. (2000b) involves decomposing the bridge dynamic system into modal coordinates, and then performing the buffeting analysis on selected modes. With the development of the finite-element method, the aerodynamic force can also be simulated on elements' nodes by introducing additional discretized aerodynamic nodal stiffness and damping (Xu et al. 1998; Ge and Zhao 2014); thus, full mode analysis can be performed on the finite-element numerical model.

The time domain approach also requires multidimensional multivariate wind fields as the input excitation. These can be simulated using the spectral superposition method (Shinozuka 1974; Deodatis 1996) or the autoregressive time series approach (Li and Kareem 1990).

With the development of high-frequency wind field monitoring systems and a deeper understanding of the nature of the wind phenomenon, the non-Gaussian features of wind turbulence have become another cause of increasing concern for modern wind-induced vibration analysis (Cao et al. 2009; Li et al. 2015). Currently, non-Gaussian wind pressure on buildings has been extensively studied (Kareem and Wu 2013; Yang and Tian 2015). The non-Gaussian nature of wind fields has been recorded in several studies (Hui et al. 2017), but the related dynamic effect through the wind–force–response wind loading chain has been of less concern in the context of flexible structures, such as long-span bridges and tall buildings. Karmakar et al. (2012) provide a case study with respect to the buffeting response of the Vincent Thomas Bridge as excited by the non-Gaussian wind field, which is based on field measurements. However, a wide range of turbulence skewness and bridge dynamic properties have not been discussed in the recent literature. At the same time, the non-Gaussian wind pressures have become further causes for concern (Kareem and Wu 2016), especially for extreme pressure prediction (Wu et al. 2020; Liu et al. 2020) and uncertainty quantification (Yang et al. 2019).

In this study, non-Gaussian wind turbulence effects on the buffeting response of bridges with different span lengths are examined based on the time domain simulation method, which are also compared with Gaussian turbulence excitation. The bridge dynamic responses induced by non-Gaussian turbulence with different skewness values are comprehensively investigated in terms of RMS and extreme values using Monte Carlo simulation, while the statistical higher-order moment and spectral characteristics of the structural response are also studied. Before applying time domain simulation to non-Gaussian turbulence-induced vibration, it should be noted that both current time domain and frequency domain methods for long-span bridges considering aeroelasticity are based on Gaussian excitations. Few studies focus on the non-Gaussian process applied to the classical linear dynamic system to derive high-order moments of responses (Gusella and Materazzi 2000; Grigoriu and Ariaratnam 1988); furthermore, theoretical or experimental methods to describe the aeroelastic force of the moving bridge deck in the non-Gaussian turbulent wind flow have not been established. Therefore, the fundamental assumption of this study is that the aeroelastic force model of Gaussian turbulence is still valid for non-Gaussian turbulence, and this assumption will be examined and discussed in this study.

Non-Gaussian Turbulence in Typhoon Climate

Non-Gaussian turbulence has been observed in large Reynolds number turbulence (Tabeling et al. 1996) and wall-bounded turbulence (Djenidi et al. 2017). A climatic model stated that nonlinear surface drag is the main reason for non-Gaussian turbulence (Monahan 2004). For example, in previous measured typhoon records, the turbulence near the typhoon center has positive skewness. Fig. 1 shows two turbulence examples and related probabilistic distributions with different skewness values from the outer region of Typhoon Bolaven (2012), measured at the Xihoumen Bridge site; Fig. 1 clearly shows that the histogram deviated from the fitted Gaussian function and that the high gust cannot be modeled using a Gaussian process.

Skewness and kurtosis present the normalized third and fourth moments of a random process, which are defined as

$$\gamma_u = \frac{\mathbb{E}\left[(u-\mu_u)^3\right]}{\sigma_u^3} \tag{1}$$

$$\kappa_u = \frac{\mathbb{E}\left[(u-\mu_u)^4\right]}{\sigma_u^4} \tag{2}$$

where γ_u = skewness; κ_u = kurtosis; u is a random process; μ_u and σ_u are the mean and standard deviation of u; and $\mathbb{E}[\ ]$ is the expectation operator.

The higher-order properties of typhoon wind turbulence distribution have not been the main concern in most previous studies. Cao et al. (2009) states that skewness and kurtosis are independent of wind speeds. Li et al. (2015) showed that skewness and kurtosis have weak correlation with turbulence intensity. In typhoon structures, the tangential airflows are expedited as the wind flow spirals into the typhoon center, owing to the shorter radius. The radial airflows are accelerated by the typhoon gradient pressure field.

Fig. 2 plots the variation of the skewness and kurtosis of typhoon wind turbulence from the wind records of four typhoons. Although a large portion of turbulence records do not exhibit clear non-Gaussian features, there are some skewed turbulence records in the typhoon wind records. More detailed information and a comprehensive analysis of typhoon wind turbulence and associated non-Gaussian features can be found in Zhao et al. (2019). This positive skewness of turbulence in a typhoon climate should be studied for engineering applications.

Theoretical Background of Time Domain Bridge Buffeting Response Analysis

Fig. 3 shows the bridge section external force and motion per unit span.

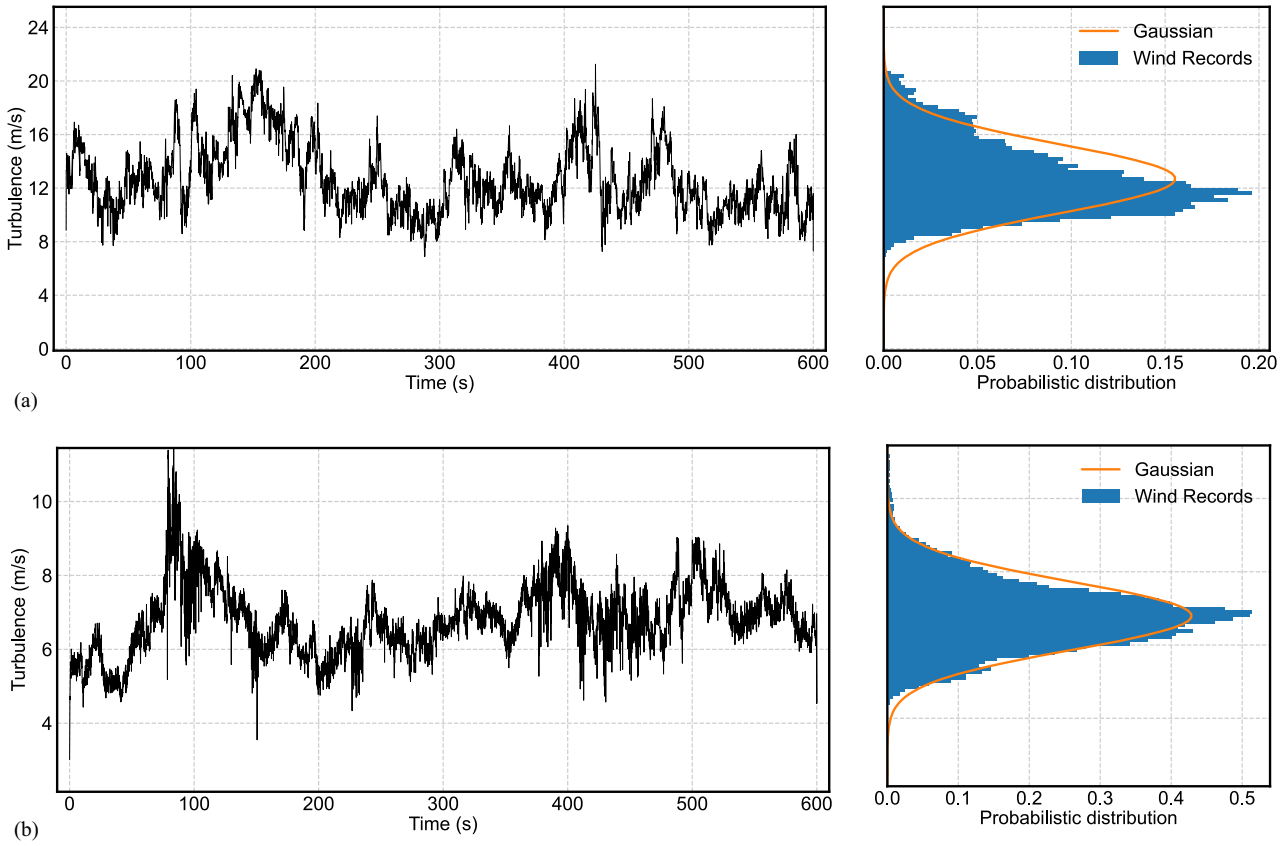

Fig. 1. Examples of positive skewed turbulence from Typhoon Bolaven (2012): (a) skewness ≈1; and (b) skewness ≈0.5.

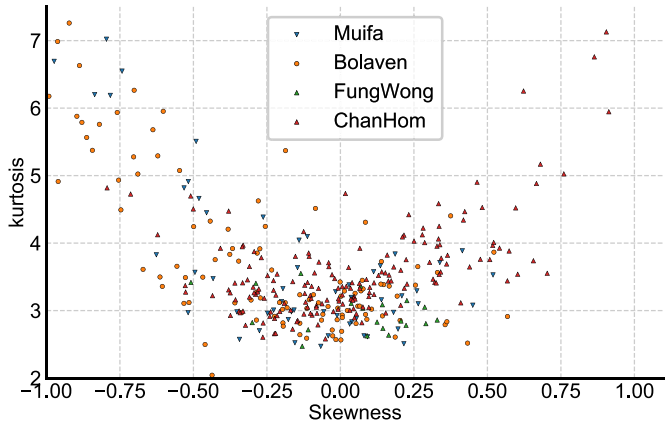

Fig. 2. Variation of turbulence skewness and kurtosis of the wind records of four typhoons.

The equation governing bridge deck motion can be expressed as

$$\mathbf{M}\ddot{\mathbf{d}} + \mathbf{C}\dot{\mathbf{d}} + \mathbf{K}\mathbf{d} = \mathbf{F}_{se} + \mathbf{F}_{b} \tag{3}$$

where **M**, **C**, and **K** are mass, damping, and stiffness matrices, respectively; **d** is the motion array consisting of the three degree-of-freedom (DOF) displacements: lateral p, vertical h, and pitching rotation α. For long-span bridges, the external excitation forces **F** normally have two parts: a self-excited aeroelastic force, $\mathbf{F}_{se}$, and a turbulence-induced aerodynamic force, $\mathbf{F}_{b}$. Both of these have three components: lift force, L_{se} and L_b; drag force, D_{se} and D_b; and torque, M_{se} and M_b.

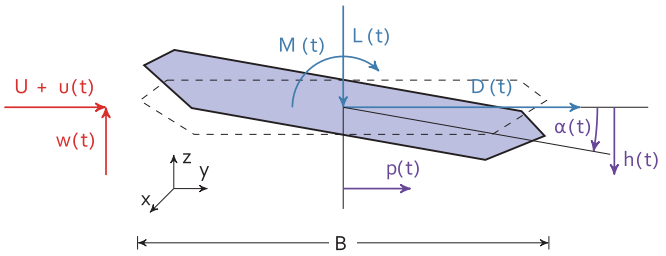

Fig. 3. Coordinates of aerodynamic force and bridge motion [the notation is given in Eq. (4)].

For harmonic motion, the self-excited forces are commonly described in the form of flutter derivatives (Scanlan 1978a):

$$L_{se} = \frac{1}{2}\rho U^2 B\left(kH_1^*\frac{\dot{h}}{U} + kH_2^*\frac{B\dot{\alpha}}{U} + kH_3^*\alpha + kH_4^*\frac{h}{B} + kH_5^*\frac{\dot{p}}{U} + kH_6^*\frac{p}{B}\right) \tag{4a}$$

$$D_{se} = \frac{1}{2}\rho U^2 B\left(kP_1^*\frac{\dot{p}}{U} + kP_2^*\frac{B\dot{\alpha}}{U} + kP_3^*\alpha + kP_4^*\frac{p}{B} + kP_5^*\frac{\dot{h}}{U} + kP_6^*\frac{h}{B}\right) \tag{4b}$$

$$M_{se} = \frac{1}{2}\rho U^2 B^2\left(kA_1^*\frac{\dot{h}}{U} + kA_2^*\frac{B\dot{\alpha}}{U} + kA_3^*\alpha + kA_4^*\frac{h}{B} + kA_5^*\frac{\dot{p}}{U} + kA_6^*\frac{p}{B}\right) \tag{4c}$$

where ρ = air density; U = mean wind speed; $k = \omega B/U$ = reduced frequency; B = bridge deck width; ω = circular frequency; and H_i^*, P_i^*, and A_i^* ($i = 1$–6) are frequency-dependent flutter derivatives.

Through Fourier transformation, Eq. (4) can be transformed into the frequency domain in matrix form, as

$$\begin{Bmatrix} L_{se} \\ D_{se} \\ M_{se} \end{Bmatrix} = \frac{1}{2}\rho U^2 \begin{bmatrix} B & & \\ & B & \\ & & B^2 \end{bmatrix} \times \begin{bmatrix} k^2(H_4^* + iH_1^*) & k^2(H_6^* + iH_5^*) & k^2(H_3^* + iH_2^*) \\ k^2(P_4^* + iP_1^*) & k^2(P_6^* + iP_5^*) & k^2(P_3^* + iP_2^*) \\ k^2(A_4^* + iA_1^*) & k^2(A_6^* + iA_5^*) & k^2(A_3^* + iA_2^*) \end{bmatrix} \times \begin{Bmatrix} h/B \\ p/B \\ \alpha \end{Bmatrix} \tag{5}$$

The flutter derivative matrix can be approximated by a rational function, as Chen et al. (2000b)

$$\begin{bmatrix} k^2(H_4^* + \iota H_1^*) & k^2(H_6^* + \iota H_5^*) & k^2(H_3^* + \iota H_2^*) \\ k^2(P_4^* + \iota P_1^*) & k^2(P_6^* + \iota P_5^*) & k^2(P_3^* + \iota P_2^*) \\ k^2(A_4^* + \iota A_1^*) & k^2(A_6^* + \iota A_5^*) & k^2(A_3^* + \iota A_2^*) \end{bmatrix} = \mathbf{A}_1 + \mathbf{A}_2(\iota k) + \mathbf{A}_3(\iota k)^2 + \sum_{l=1}^{m} \frac{\mathbf{A}_{l+3}\iota k}{\iota k + d_l} \tag{6}$$

where $\mathbf{A}_1$, $\mathbf{A}_2$, $\mathbf{A}_3$, $\mathbf{A}_{l+3}$, and d_l are all frequency-independent variables and can be found by using the least-squares method.

Through inverse Fourier transformation, the self-excited force is rewritten as

$$\begin{Bmatrix} L_{se} \\ D_{se} \\ M_{se} \end{Bmatrix} = \frac{1}{2}\rho U^2 \begin{bmatrix} B & & \\ & B & \\ & & B^2 \end{bmatrix} \times \left[\mathbf{A}_1\mathbf{d} + \mathbf{A}_2\frac{B}{U}\dot{\mathbf{d}} + \mathbf{A}_3\frac{B^2}{U^2}\ddot{\mathbf{d}} + \sum_{l=1}^{m} \boldsymbol{\phi}_l(t) \right] \tag{7a}$$

$$\dot{\boldsymbol{\phi}}_l(t) = -\frac{d_l U}{B}\boldsymbol{\phi}_l(t) + \mathbf{A}_{l+3}\dot{\mathbf{d}} \tag{7b}$$

where $\boldsymbol{\phi}_l(t)$ = aerodynamic phase lag.

The turbulence-dependent buffeting forces per unit span are normally expressed as in Scanlan (1978b)

$$L_b(t) = \frac{1}{2}\rho U^2 B\left[2C_L\chi_{L_{bu}}\frac{u(t)}{U} + (C_L' + C_D)\chi_{L_{bw}}\frac{w(t)}{U}\right] \tag{8a}$$

$$D_b(t) = \frac{1}{2}\rho U^2 B\left[2C_D\chi_{D_{bu}}\frac{u(t)}{U} + C_D'\chi_{D_{bw}}\frac{w(t)}{U}\right] \tag{8b}$$

$$M_b(t) = \frac{1}{2}\rho U^2 B^2\left[2C_M\chi_{M_{bu}}\frac{u(t)}{U} + C_M'\chi_{M_{bw}}\frac{w(t)}{U}\right] \tag{8c}$$

where C_L, C_D, and C_M are lift, drag, and moment coefficients, respectively; $C_D' = dC_D/d\alpha$; $C_L' = dC_L/d\alpha$; $C_M' = dC_M/d\alpha$; and $\chi_{L_{bu}}$, $\chi_{L_{bw}}$, $\chi_{D_{bu}}$, $\chi_{D_{bu}}$, $\chi_{M_{bu}}$, and $\chi_{M_{bw}}$ are aerodynamic admittance functions, which are frequency-dependent. Admittance functions can also be approximated by rational functions. Take $\chi_{L_{bu}}$ as an example:

$$\chi_{L_{bu}} = A_{u,l} + \sum_{l=1}^{m_u} \frac{A_{u,l+1}\iota\omega}{\iota\omega + d_{u,l}} \tag{9}$$

where $A_{u,l}$, $A_{u,l+1}$, and $d_{u,l}$ are all frequency-independent variables.

Transferring these equations into the time domain, the lift buffeting force cause by turbulence u is

$$L_{bu}(t) = \frac{1}{2}\rho U^2 B 2C_L\left[\left(A_{u,l} + \sum_{l=1}^{m_u} A_{u,l+1}\right)\frac{u(t)}{U} - \sum_{l=1}^{m_u}\frac{d_{u,l}U}{B}\phi_{u,l}(t)\right] \tag{10a}$$

$$\dot{\phi}_{u,l}(t) = -\frac{d_{u,l}U}{B}\phi_{u,l}(t) + A_{u,l+1}\frac{u(t)}{U} \tag{10b}$$

Other buffeting force components can be expressed similarly and are omitted here for brevity.

For time domain analysis, the buffeting forces should be discretized onto each element. The joint acceptance function expresses the spanwise turbulence coherence. Taking $L_{bu}(t)$ as an example, the associated joint acceptance functions are normally expressed in the frequency domain as

$$J_{L_{bu}}^2(\omega) = \frac{1}{L^2}\int_0^L\int_0^L \mathrm{coh}_{L_{bu}}(x_1, x_2; \omega)\, dx_1\, dx_2 \tag{11}$$

where L = element length.

The function $J_{L_{bu}}^2(\omega)$ can then also be approximated by a rational function in the same way as the admittance function in Eq. (9).

However, as bridge spans have continuously increased in recent years, the numbers of elements are also increasing. As a result, the computing times consumed in evaluating $\phi_{u,l}(t)$ for the admittance function and joint acceptance function are also increasing exponentially. In this study, it is proposed that the admittance function and joint acceptance function can be analyzed together with one rational function approximation:

$$\chi_{L_{bu}}(\omega)J_{L_{bu}}(\omega) = A_{u,l} + \sum_{l=1}^{m_u} \frac{A_{u,l+1}\iota\omega}{\iota\omega + d_{u,l}} \tag{12}$$

Thus, the computing time for calculating the buffeting force can be reduced by half using this method.

For linear structures, modal decomposition is normally used to reduce system order and increase computational efficiency:

$$\mathbf{M_q}\ddot{\mathbf{q}} + \mathbf{C_q}\dot{\mathbf{q}} + \mathbf{K_q}\mathbf{q} = \mathbf{Q}_{se} + \mathbf{Q}_b \tag{13}$$

where $\mathbf{M_q} = \boldsymbol{\Phi}^T\mathbf{M}\boldsymbol{\Phi}$ = modal generalized mass; $\mathbf{C_q} = \boldsymbol{\Phi}^T\mathbf{C}\boldsymbol{\Phi}$ = modal generalized damping; $\mathbf{K_q} = \boldsymbol{\Phi}^T\mathbf{K}\boldsymbol{\Phi}$ = modal generalized stiffness; $\mathbf{Q}_{se} = \boldsymbol{\Phi}^T\mathbf{F}_{se}$ = generalized self-excited force; $\mathbf{Q}_b = \boldsymbol{\Phi}^T\mathbf{F}_b$ = generalized buffeting force; and $\boldsymbol{\Phi}$ is the mode shape matrix.

Finally, the generalized motion equation can be expressed by the state-space equation:

$$\dot{\mathbf{Y}} = \mathbf{A}\mathbf{Y} + \mathbf{B}\mathbf{Q}_b \tag{14}$$

where

$$\mathbf{Y} = \begin{Bmatrix} \mathbf{q} \\ \dot{\mathbf{q}} \\ \mathbf{q}_{se,1} \\ \vdots \\ \mathbf{q}_{se,m} \end{Bmatrix} \tag{15a}$$

$$\mathbf{A} = \begin{bmatrix} \mathbf{0} & \mathbf{I} & \mathbf{0} & \cdots & \mathbf{0} \\ -\bar{\mathbf{M}}^{-1}\bar{\mathbf{K}} & -\bar{\mathbf{M}}^{-1}\bar{\mathbf{C}} & \frac{1}{2}\rho U^2 \bar{\mathbf{M}}^{-1} & \cdots & \frac{1}{2}\rho U^2 \bar{\mathbf{M}}^{-1} \\ \mathbf{0} & \mathbf{A}_{4,q} & -\frac{U}{B} d_1 \mathbf{I} & \cdots & \mathbf{0} \\ \vdots & \vdots & \vdots & \ddots & \vdots \\ \mathbf{0} & \mathbf{A}_{3+m,q} & \mathbf{0} & \cdots & -\frac{U}{B} d_m \mathbf{I} \end{bmatrix} \tag{15b}$$

$$\mathbf{B} = \begin{bmatrix} \mathbf{0} \\ \bar{\mathbf{M}}^{-1} \\ \mathbf{0} \\ \vdots \\ \mathbf{0} \end{bmatrix} \tag{15c}$$

$$\bar{\mathbf{M}} = \mathbf{M}_{\mathbf{q}} - \frac{1}{2}\rho B^2 \mathbf{A}_{3,\mathbf{q}} \tag{15d}$$

$$\bar{\mathbf{C}} = \mathbf{C}_{\mathbf{q}} - \frac{1}{2}\rho B U \mathbf{A}_{2,\mathbf{q}} \tag{15e}$$

$$\bar{\mathbf{K}} = \mathbf{K}_{\mathbf{q}} - \frac{1}{2}\rho U^2 \mathbf{A}_{1,\mathbf{q}} \tag{15f}$$

where $\mathbf{A}_{i,\mathbf{q}} = \mathbf{\Phi}^T \mathbf{A}_i \mathbf{\Phi}$ ($i = 1$–m) indicates the generalized aerodynamic frequency-independent coefficients.

Verification of Time Domain Analysis of Wind-Induced Bridge Vibration

The time domain simulation methodology used in this study is explained in detail and verified using the Golden Gate Bridge model in Jones and Scanlan (2001) through comparison against the frequency domain results in this section.

Flutter Analysis

From the state-space time domain bridge vibration equation [Eq. (14)], the bridge flutter critical wind speed can be estimated by complex eigenvalue analysis (Chen et al. 2000b). From the bridge structural and aerodynamic parameters shown in the previous section, the critical flutter wind speed is 62.5 m/s. Ignoring the buffeting force, bridge vibration time series in laminar flow speeds can be calculated using Eq. (14). Fig. 4 shows the bridge vibration (with the same initial vibration speeds) at quarter span ($x = l/4$) for wind speeds of 30 and 65 m/s, respectively.

For $U = 30$ m/s, vibrations in both directions decay to zero, owing to the structural damping effects. However, when $U = 65$ m/s, aeroelastic damping exceeds structural damping, and both vertical and torsional vibrations continue increasing, which indicates onsite fluttering.

It should be noted that the critical flutter wind speed derived by the direct frequency-based method (Jones and Scanlan 2001) is 61.9 m/s, which exhibits only 0.9% difference in comparison with the time domain aerodynamic approximation method.

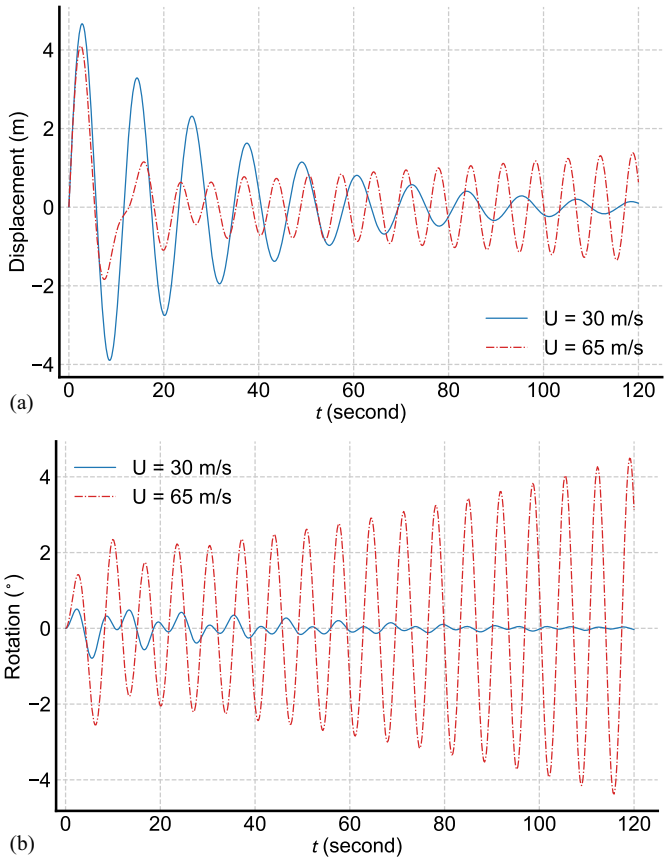

Fig. 4. Examples of bridge vibration at quarter span ($x = l/4$) in laminar flow: (a) vertical displacement; and (b) rotation.

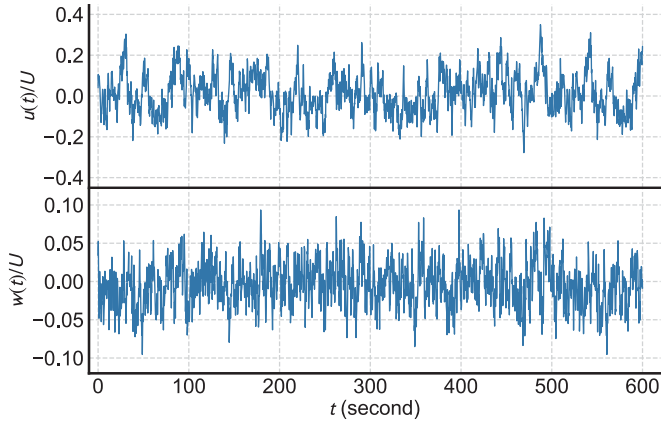

Fig. 5. Example of simulated wind fluctuations ($U = 30$ m/s).

Buffeting Analysis

To verify the effectiveness of the time domain buffeting analysis method, a detailed comparison against frequency domain results was performed. At first, the multivariate Gaussian turbulence time history was generated using Eq. (18), and the along-wind and vertical turbulence with a 600-s duration at the middle span, as an example, at a mean wind speed of 30 m/s are shown in Fig. 5. The power spectrum

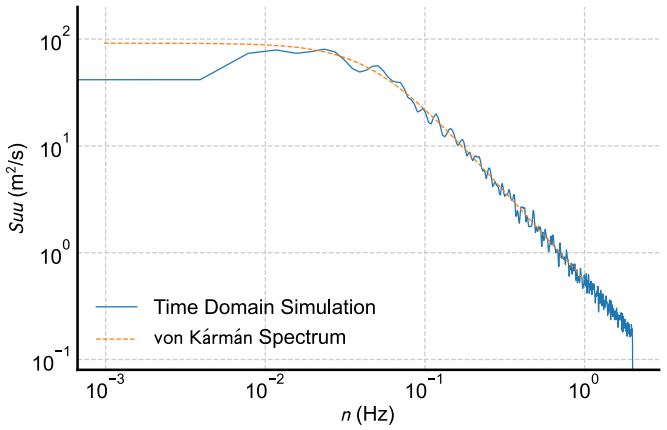

Fig. 6. Comparison of turbulence spectra.

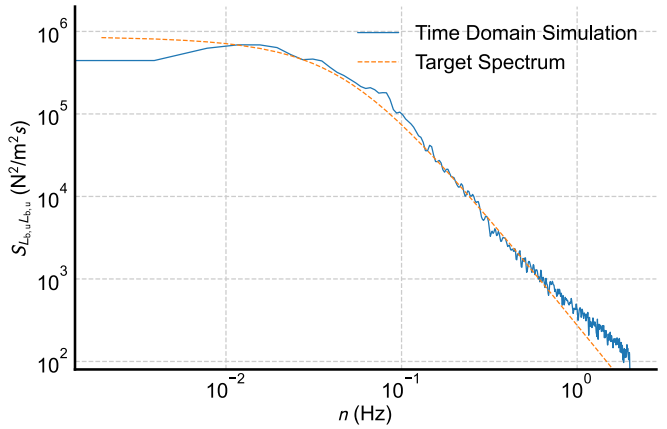

Fig. 7. Comparison of vertical buffeting force induced by along-wind turbulence on unit span.

density of along-wind turbulence u in the time domain is plotted in Fig. 6, which matches the von Kármán spectra model in the frequency domain. The comparison of vertical turbulence w is omitted for brevity.

Next, the buffeting force on the unit span considering the chordwise aerodynamic admittance can be evaluated by Eq. (10) with $m_u = 2$. As an example, the power spectrum density values of vertical buffeting forces induced by along-wind turbulence L_{bu} are illustrated in Fig. 7; these are also comparable to the values directly derived in the frequency domain.

For the buffeting force on the discretized bridge section element, the spanwise turbulence coherence in Eq. (11) must also be included with chordwise aerodynamic admittance. The simplified method proposed in Eq. (12) combines spanwise and chordwise aerodynamic admittance in one set of rational function parameters. The buffeting force L_{bu} on the element at the middle span is plotted in Fig. 8 and is comparable to the frequency domain results. Excellent similarity can be found in Fig. 8, except for the high-frequency region ($n > 0.8$ Hz). This deviation can be improved by increasing the rational function number m_w, but a larger value of m_w will dramatically increase computation time.

By integrating the buffeting forces on all elements and transforming them into modal coordinates, the generalized buffeting forces $\mathbf{Q}_b$ on the first vertical and torsional modes can be determined, as shown in Fig. 9. Substituting the buffeting forces into the state-space formula in Eq. (14), the bridge buffeting response

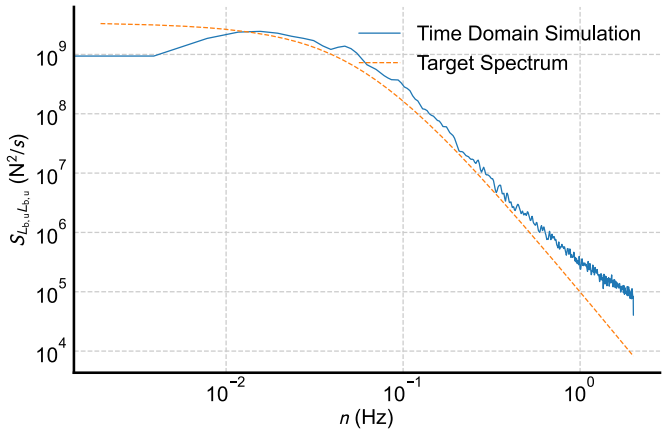

Fig. 8. Comparison of vertical buffeting force induced by along-wind turbulence on section element.

can be calculated in model coordinates. Fourth Runge–Kutta methods are used in this study to solve the time differential equations.

Fig. 10 shows a comparison of the power spectrum density of the structural vertical $h(x = l/4)$ and torsional response $\alpha(x = l/4)$ at quarter span (owing to antisymmetric mode shapes) from the time domain analysis and frequency domain approach (Jones and Scanlan 2001). (In the following sections of this paper, $h(x = l/4)$ and $\alpha(x = l/4)$ are simplified as h and α, respectively.) Both resonant responses from the two methods in the vertical and torsional directions match at the primary modal frequency; this verifies the accuracy and effectiveness of the time domain buffeting analysis methods used in this study. However, there are differences in resonant response at the secondary modal frequency, owing to aerodynamic coupling; this might be caused by the signal processing errors from Welch's method (Welch 1967).

Description of Long-Span Suspension Bridge Prototypes

In this study, six different finite-element models of suspension bridges with main spans of 1,000, 1,200, 1,400, 1,600, 1,800, and 2,000 m were built to study non-Gaussian turbulence effects on the bridge buffeting response. Because of the different bridge spans, the bridge tower heights also varied. Apart from the bridge spans and tower heights, other structural parameters and aerodynamic factors related to the bridge section remained consistent for the six different models. The bridge and coordinates are shown in Fig. 11. The consistent parameters for the different bridge models are shown in Table 1, in which the aerodynamic parameters are extracted from Chen et al. (2000b).

The finite-element analysis was conducted using the ANSYS platform. Three-dimensional Euler beam elements (BEAM188) with axial stiffness were used to model the bridge towers with rigid lateral arms. Tensile link (LINK180) elements were employed to model the suspended cables and hangers. The main bridge girder was also modeled using Euler beam elements (BEAM188) and connected to hangers through a rigid "fishbone" framework (Ko et al. 1998). The bridge girders and suspension cables were discretized at the hanger locations. Because the bridge towers had a uniform section, the towers were discretized at the elevations of bridge girders and horizontal connectors. The bases of bridge towers were considered as fixed ends, and the two free ends of bridge girders as vertically supported. Additionally, the bridge girders and towers were connected through the

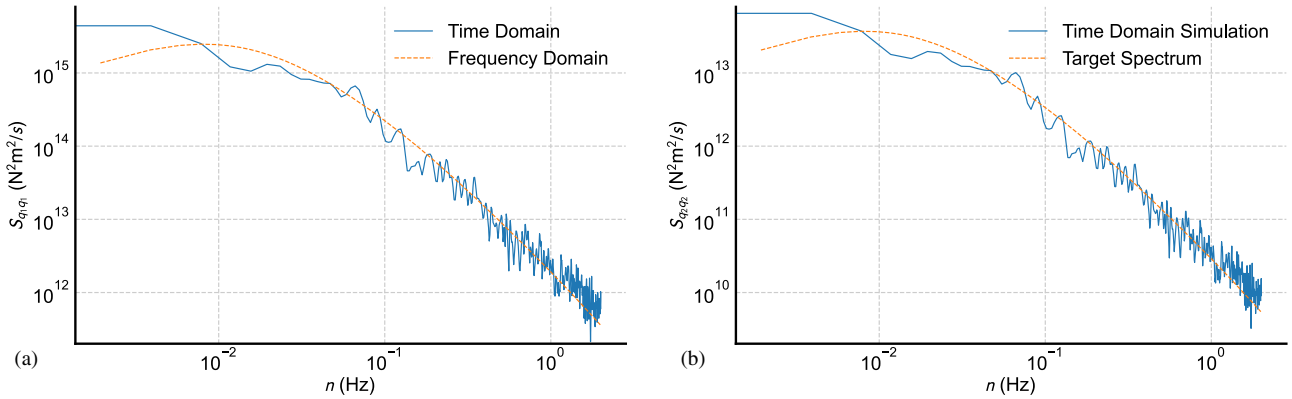

Fig. 9. Comparison of generalized buffeting forces: (a) Mode 1; and (b) Mode 2.

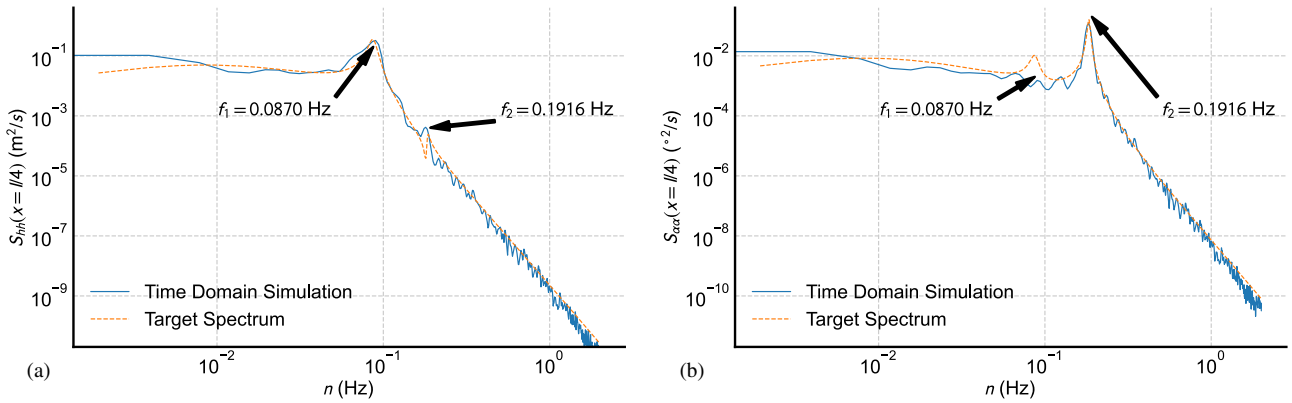

Fig. 10. Comparison of buffeting response at bridge quarter span $x = l/4$: (a) lift 1; and (b) rotation.

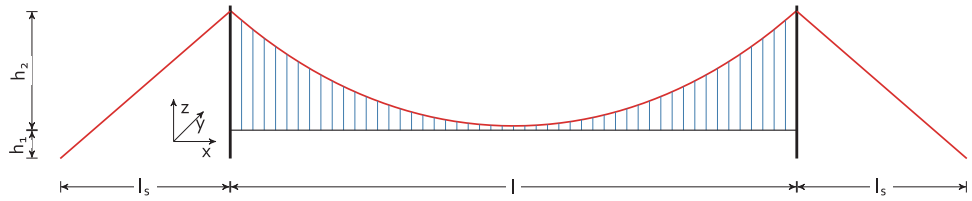

Fig. 11. Elevation view of the bridge geometries.

longitudinal axis with vertical restrictions. Large displacement effects were considered, and the Newton–Raphson algorithm was employed to calculate the geometric nonlinearity. Equivalent initial strain was applied to suspension cables and hangers as the pre-tension in link elements.

The typical eigenvalue analysis was used to calculate the bridge's fundamental frequency and associated mode shapes. The buffeting response was induced by turbulent wind, and, taking Fig. 6 as an example, most of its energy was concentrated within the low-frequency band and then decayed rapidly in the high-frequency inertial subrange (Simiu and Yeo 2019).

Furthermore, to compare the different non-Gaussian turbulence effects on the background and the resonant component of the structural response, only the selected first vertical and torsional modes of the modeled bridges were considered in this study; this is common practice for a bridge buffeting response (Seo and Caracoglia 2012, 2013). For long-span suspension bridges with streamlined sections, the along-wind responses for both bridge girders and cables have been of less concern because of the high width-to-depth ratio.

The fundamental frequencies of six bridge models with different spans are given in Table 2 with bridge span and tower configurations. It should be noted that, owing to the long bridge span, both of the first vertical and torsional mode shapes are antisymmetric for all analyzed bridge models with six span lengths. The dependences of the first vertical bending and rotational frequencies on the main span length of long-span bridges are plotted in Fig. 12.

The parameters H_1^* to H_4^* and A_1^* to A_4^* were evaluated using the Theodorsen function (Theodorsen 1935); other flutter derivatives were not used in this study. The values of $\chi_{L_{bu}}$, $\chi_{L_{bw}}$, $\chi_{M_{bu}}$, and $\chi_{M_{bw}}$ were given by the Sears function (Sears 1941). It should be noted that the aerodynamic admittance function, which is normally applied for Gaussian turbulence, was also assumed to be valid for non-Gaussian turbulence in this study.

The along-wind and vertical turbulence spectra were assumed to follow the von Kármán and Panofsky types, respectively, as

$$\frac{nS_{uu}}{\sigma_u^2} = \frac{4f_u}{\left(1 + 70.78f_u^2\right)^{5/6}} \tag{16a}$$

Table 1. Consistent structural parameters of six bridge models

Parameters	Values
Main span	1,000, 1,200, 1,400, 1,600, 1,800, 2,000
Sag/span ratio	1/11
Deck width B (m)	36
Deck thickness D (m)	4
Suspender gap (m)	20
Mass per unit length m (kg/m)	22,000
Mass moment of inertia long longitudinal axis per unit length I (kg · m^2/m)	2,210,000
Area of bridge section (m^2)	1.11
Area moment of inertia I_x, I_z, I_y (m^4)	5.5, 94, 2.64
Structural damping ratio ξ	0.005
Air density ρ (kg/m^3)	1.25
Lift coefficient C_L	0.0942
Drag coefficient C_D	0.3042
Moment coefficient C_M	0.0104
Lift coefficient derivative $dC_L/d\alpha$	1.9050
Drag coefficient derivative $dC_D/d\alpha$	0
Moment coefficient derivative $dC_M/d\alpha$	0.2717

Table 2. Bridge span, tower height, and parameters of six bridge models

l (m)	l_s (m)	h_1 (m)	h_2 (m)	f_h (Hz)	f_α (Hz)
1,000	300	130	32.5	0.1300	0.3519
1,200	400	156	39.0	0.1150	0.2870
1,400	450	182	45.5	0.1042	0.2442
1,600	500	208	52.0	0.0962	0.2152
1,800	600	234	58.5	0.0898	0.1926
2,000	700	260	68.0	0.0844	0.1751

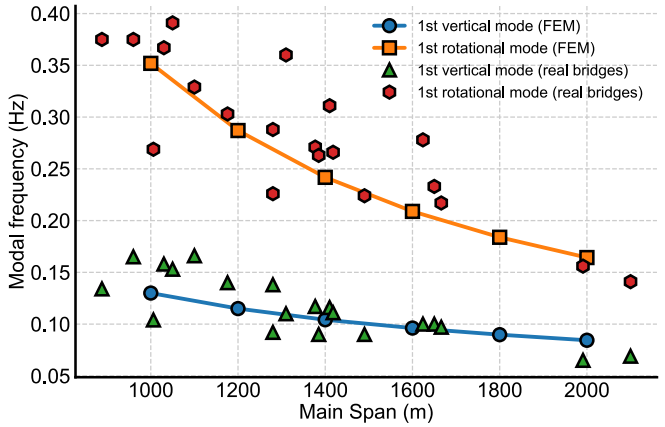

Fig. 12. Dependences of long-span bridge vertical bending and rotational modal frequencies on main span lengths.

$$\frac{nS_{ww}}{u_*^2} = \frac{3.36f_z}{1+10f_z^{5/3}} \tag{16b}$$

where $f_u = nL_u/U$ is the reduced frequency dependent on turbulence integral length; $f_z = nz/U$ is the reduced frequency dependent on elevation; and u_* is assumed as $u_*^2 = \sigma_u^2/6$. In this study, the turbulence intensity was assumed as 0.1 for both I_u and I_w, and the integral length L_u and L_w dependence on intensity were assumed to follow the findings in Zhao et al. (2019). The definitions of turbulence intensity I_u and I_w and integral length L_u and L_w can be found in Zhao et al. (2019) and Simiu and Scanlan (1996).

The spanwise correlation of buffeting forces was assumed to be the same as the turbulence correlation. Both along-wind and vertical turbulence coherence functions are expressed as Simiu and Scanlan (1996)

$$\mathrm{coh}(x_1, x_2; \omega) = \exp\left(-\frac{c\omega|x_1 - x_2|}{2\pi U}\right) \tag{17}$$

where c is the decay coefficient and is assumed to be 10, and x_1 and x_2 are the coordinates of two points of interest along the bridge span.

Simulation of Bridge Buffeting Responses Induced by Gaussian and Non-Gaussian Turbulence

Simulation of Correlated Gaussian and Non-Gaussian Wind Fields

According to the methods presented in Zhao et al. (2019), the multivariate wind field distributed at discretized nodes along the bridge span with Gaussian turbulence can be generated using the spectral representation method based on the Shinozuka equation:

$$u_i(t) = \sqrt{4\pi\Delta n}\sum_{m=1}^{i}\sum_{l=1}^{N}|H_{im}(n_{ml})|\cos(2\pi n_{ml}t - \theta_{im}(n_{ml}) + \Phi_{ml}) \tag{18}$$

where i denotes the ith node of the discretized random wind field; m is the node number before i; N = number of evaluated frequency points, which should be sufficiently large; l is the index for discretized frequency; $\Delta n = n_{\mathrm{up}}/N$ = frequency increment; n_{up} = upper cutoff frequency; Φ_{ml} = independent random phase angle; H_{im} is derived from Cholesky's decomposition of S_{uu}; and θ_{im} is the complex angle of H_{im}. Meanwhile, the non-Gaussian turbulence is simulated by the translation process established by Grigoriu (1984) to ensure the consistency of the turbulence spectrum as well as the turbulence intensity.

Fig. 13 illustrates 600 s time series of the along-wind turbulence at one node for three different skewness values $\gamma = 0.5$, 1.0, 1.5. The dependence of kurtosis κ on skewness γ is assumed to follow the relationship given in Zhao et al. (2019). For comparison purposes, the random phase angle Φ_{ml} in Eq. (18) is the same for Gaussian and non-Gaussian turbulence. Because implementations of Φ_{ml} are different in each simulation, the vibration results contain unavoidable randomness; this will be investigated later.

Each non-Gaussian turbulence illustration in Fig. 13(a) demonstrates the positive skewness features, while the turbulence spectrum features with different skewness values are identical, as demonstrated in Fig. 13(b). The coherence features of turbulence can also meet the requirements; this is omitted here for brevity and can be found in Zhao et al. (2019). The vertical turbulence skewness is assumed to be the same as the along-wind turbulence, and the illustration is omitted.

From Fig. 13(a), it can be found that, for non-Gaussian turbulence with large skewness, more frequent high-speed gusts are generated in the turbulence time series, as shown in the actual typhoon wind records. At the same time, the turbulence spectrum (S_{uu}, S_{ww}) and intensity (I_u, I_w) maintain the same values as shown in Fig. 13(b); this has been demonstrated in Yang and Gurley (2015) and Gioffre et al. (2000). This may change the

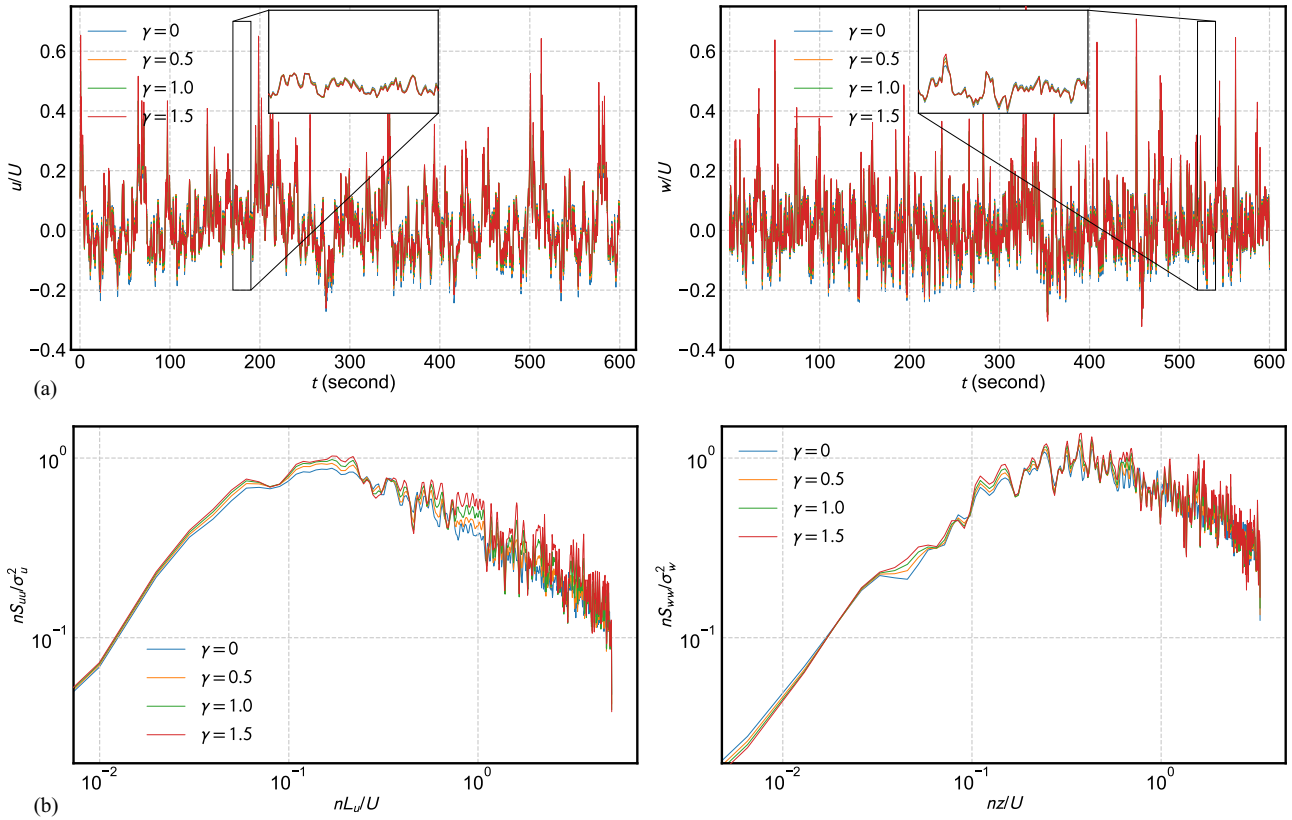

Fig. 13. Simulated Gaussian and non-Gaussian turbulence with three different skewness values: (a) time domain; and (b) frequency domain.

structural response accordingly, which will be presented and discussed in detail in the next section.

Bridge Buffeting Response Induced by Gaussian and Non-Gaussian Turbulence

For demonstration purposes, the bridge buffeting responses in the vertical and rotational directions excited by Gaussian and non-Gaussian turbulence at 30 m/s mean wind speeds for six different bridge spans (listed in Table 1) are plotted in Fig. 14.

For each bridge span, the bridge vibration time series induced by non-Gaussian turbulence with skewness $\gamma = 1$ are compared against the corresponding buffeting response induced by Gaussian turbulence $\gamma = 0$ in Fig. 14. Both vertical and rotation buffeting undergo similar periodic movements. As shown in Table 1, for longer bridge spans, both vertical and rotational buffeting responses increase in correspondence with bridge span growth. However, during most vibration periods, non-Gaussian turbulence tends to generate a larger peak response for different scenarios.

Taking the bridge span $l = 2{,}000$ m shown in Fig. 14 as an example, the vertical RMS response excited by non-Gaussian turbulence with skewness $\gamma = 1$ is 7.01% larger than the corresponding RMS response excited by Gaussian turbulence. For the rotational response, the increment ratio is 4.58%. To further investigate the vibration spectrum from a different frequency range, power spectral density values of vertical and rotational response induced by Gaussian and non-Gaussian turbulence ($\gamma_{u,w} = 1$) are plotted in Fig. 15 for bridges with different span lengths, in which both vertical and rotational frequencies decrease because of negative aerodynamic stiffness.

The spectral analysis in Fig. 15 shows that skewed turbulence in the frequency domain can affect both background response and resonant response around the bridge fundamental mode frequency. Furthermore, it demonstrates that skewed turbulence can cause a greater response in terms of RMS value, which can also induce a larger peak response.

Comparing the response spectra from bridges with different span lengths in Fig. 15, it is clear that, for the same wind speed ($U = 30$ m/s), the resonant response is increasing, compared with background response, in the rotational direction with longer bridge spans. In the vertical direction, this trend reverses.

Statistical Analysis of Bridge Buffeting Induced by Gaussian and Non-Gaussian Turbulence

One single time domain buffeting response simulation result illustrated in the previous section cannot fully represent the general regulation for the non-Gaussian turbulence effects. Thus, statistical analysis of the bridge buffeting response was implemented.

To fully compare the buffeting responses induced by non-Gaussian turbulence with different skewness values, a Monte Carlo simulation with sample size of 2,000 was carried out in this study. Furthermore, non-Gaussian turbulence with two different additional skewness parameters ($\gamma_{v,w} = 0.5$, 1.5) was included, to examine the different skewness effect.

Fig. 16 shows the RMS value distribution of vertical and torsional buffeting response for a bridge span l of 1,200 m and a wind speed U of 30 m/s. For comparison, all RMS responses were normalized to the averaged value of RMS responses induced by Gaussian turbulence ($\bar{\sigma}_{h,0}$ or $\bar{\sigma}_{\alpha,0}$). It is clearly indicated that more intense turbulence causes a larger buffeting response in terms of averaged RMS values.

Turbulence with greater skewness will generally increase the RMS response in both vertical and torsional directions, and the variances of the RMS response also become larger for heavily skewed

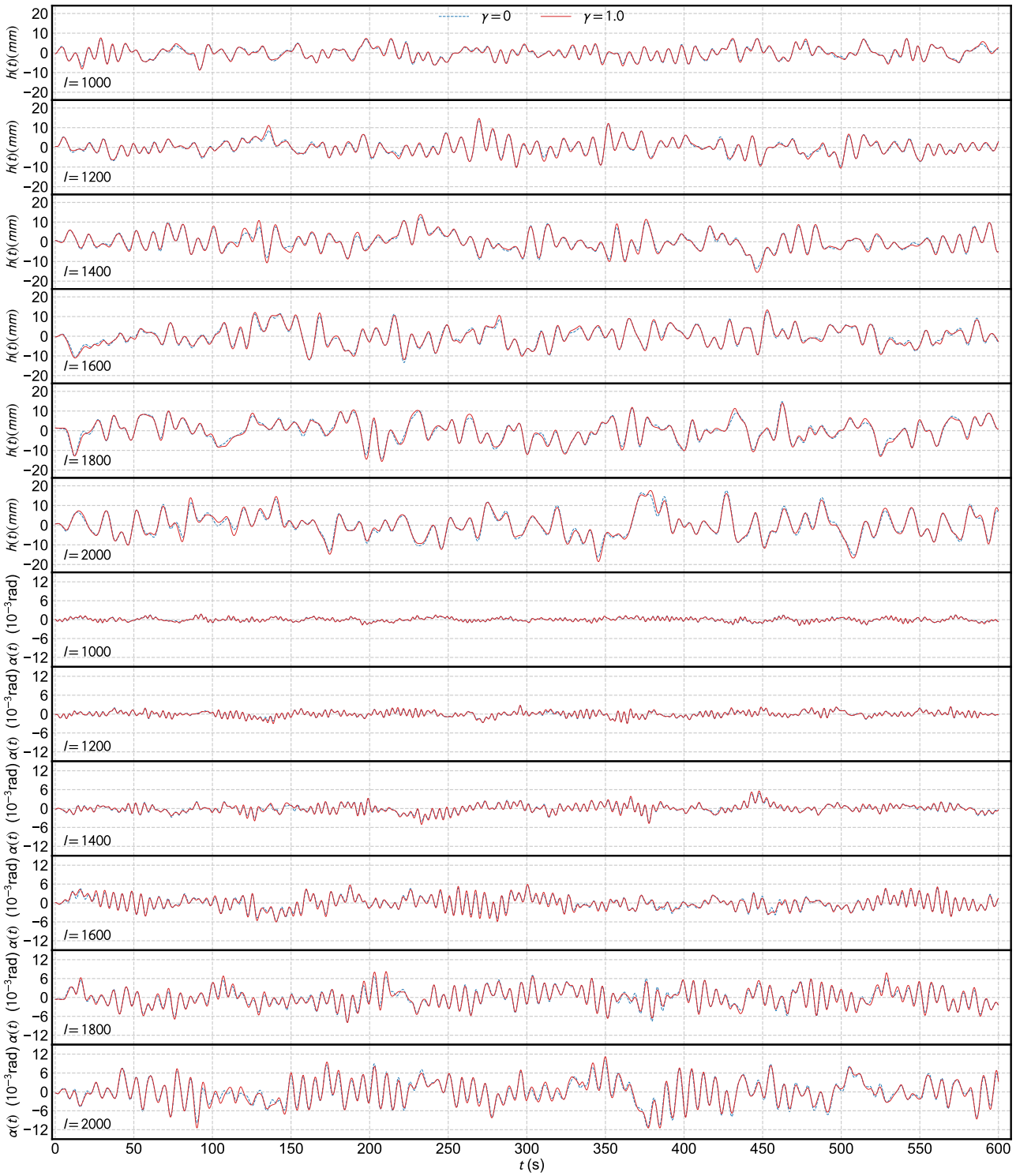

Fig. 14. Comparison of Gaussian and non-Gaussian turbulence-induced buffeting responses ($U = 30$ m/s, $\gamma_{u,w} = 1$).

turbulence. The chi-square distribution, expressed as

$$f(x; k, \sigma) = \frac{(x/\sigma)^{k-1} \exp\left[-(x/\sigma)^2/2\right]}{2^{k/2-1}\Gamma(k/2)} \tag{19}$$

where $\Gamma()$ is the gamma function, was employed to fit the RMS buffeting response; Fig. 16 shows that they match well.

To investigate the structural fundamental frequency effect on the non-Gaussian turbulence-induced buffeting response, Fig. 17 plots the RMS response for the same conditions as Fig. 16, except that bridge span $l = 1{,}800$ m. A comparison between the RMS distributions in the two different bridge spans shows that the distributions of $\bar{\sigma}_{h,\gamma}/\bar{\sigma}_{h,0}$ and $\bar{\sigma}_{\alpha,\gamma}/\bar{\sigma}_{\alpha,0}$ are almost identical, and the turbulence skewness effect on the buffeting response is similar to those of structures with different dynamic properties.

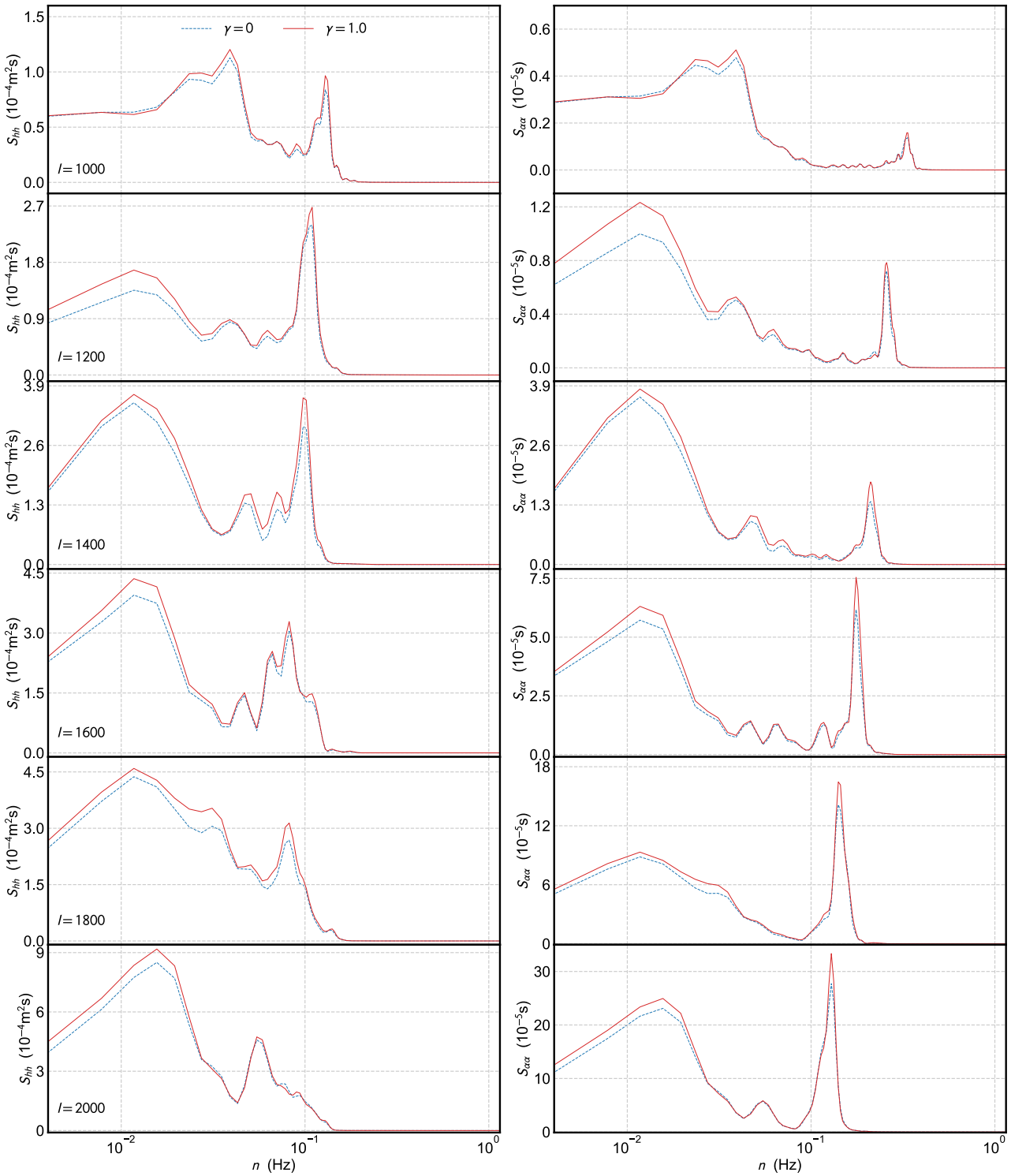

Fig. 15. Spectrum comparison of Gaussian and non-Gaussian turbulence-induced buffeting responses ($U = 30$ m/s, $\gamma_{u,w} = 1$).

Next, the relationship between the distribution of RMS buffeting response, wind speed, U and bridge span l was investigated. Fig. 18 uses error bars with 95% intervals to indicate the RMS buffeting response distribution for different values of U and l. When wind speeds are normalized to the structural fundamental frequency (f_h and f_α for vertical and rotational, respectively) and bridge width B, the change of the averaged RMS vertical response with the normalized wind speeds can be fitted to a parabola, while the averaged rotational vertical response is a cubic function of normalized wind speeds $U/f_\alpha B$. With the same procedure, the fitted parabolas and cubic curves for non-Gaussian turbulence with three different skewness values are plotted in Fig. 19(a). Taking the RMS response increasing curve as the baseline, the ratio of non-Gaussian turbulence-caused response $\sigma_{h,\gamma}$ and $\sigma_{\alpha,\gamma}$ to the baseline response induced by Gaussian turbulence $\sigma_{h,0}$ and $\sigma_{\alpha,0}$, plotted in Fig. 19(b), demonstrates that higher skewed turbulence would lead to a greater RMS buffeting response in terms of the mean value. The ratio decreases with mean wind speeds because self-excitation response, which is less affected by turbulence skewness, gradually becomes the dominant part in comparison with turbulence-induced vibration.

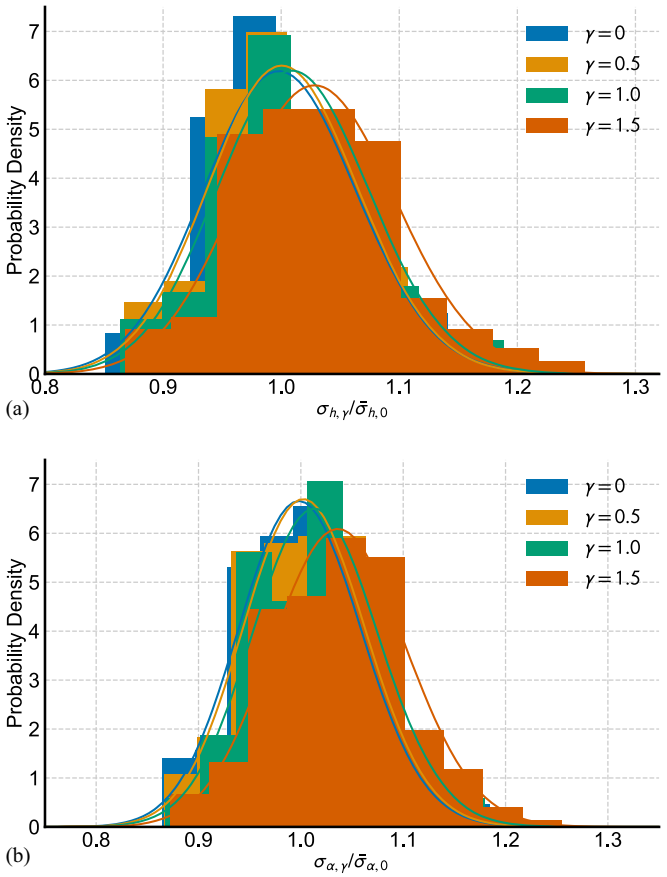

Fig. 16. Increasing RMS responses of 1,200 m span bridge induced by non-Gaussian turbulence with larger skewness ($U = 30$ m/s): (a) vertical response; and (b) torsional response.

For the non-Gaussian turbulence-induced vibration, it is also interesting to examine the non-Gaussian characteristics of buffeting response and to identify whether the non-Gaussian properties will transfer from external excitation to response. Fig. 20 shows the correlated skewness and kurtosis distribution of the vertical and torsional buffeting responses for the case with $U = 30$ m/s and $l = 1{,}800$ m. Distribution results show that the skewness of response in both the vertical and torsional directions mostly lies within the range $(-0.5, 0.5)$ and that the kurtosis mostly lies within the range $(2.5, 3.5)$. The narrow range of skewness and kurtosis indicates that the response induced by skewed turbulence remains a Gaussian process because the inertial force and restoring force in Eq. (3), rather than the external excitation, control the bridge vibration. Meanwhile, the skewness and kurtosis distributions of bridge buffeting responses excited by turbulence with different skewness values are identical. In summary, these results demonstrate that the non-Gaussian nature of the turbulence will not transfer to the response. This also confirms that the Scanlan bridge unsteady self-excited force formulation in Eq. (4) can also be applied to non-Gaussian turbulence-induced buffeting.

Extreme Response of Bridge Buffeting Induced by Gaussian and Non-Gaussian Turbulence

In addition to RMS responses, it is also necessary to examine the non-Gaussian turbulence effects on the extreme buffeting responses of long-span bridges. Similar to Fig. 18, the maximum buffeting responses induced by Gaussian turbulence from 200 simulated 10-min time intervals were extracted, and the related distributions of peak buffeting response for various wind speeds and bridge spans are plotted in Fig. 21. Parabolas and cubic curves were used to fit the relationships between normalized wind speeds and peak vertical and rotational buffeting responses, respectively.

Fig. 22 also plots the fitted increasing curves of peak buffeting response induced by non-Gaussian turbulence with three different skewness values. As for the RMS response, parabolas and cubic curves were employed to fit the increasing curves for vertical and rotational responses, respectively. Fig. 22 also shows that the effect of skewness of non-Gaussian turbulence can enlarge the peak buffeting responses.

In addition to extreme response, it is also worth investigating the peak factor of g in different skewed turbulence-induced vibrations:

$$h_{\max} = g_h \sigma_h \tag{20a}$$

$$\alpha_{\max} = g_\alpha \sigma_\alpha \tag{20b}$$

where g_h and g_α are the peak factors for vertical and torsional responses, respectively.

Fig. 23 presents box plots of g_h and g_α for bridge buffeting with different turbulence skewnesses, showing that larger skewed turbulence can also marginally increase the peak factors. For Gaussian turbulence, both g_h and g_α are approximately 3.1, and their distributions widely lie within the range 2.5–4.0. For non-Gaussian turbulence with skewness of 1.5, the median of g_h is 3.25, and its range also increased to 2.6–4.4. The peak factors for torsional response also exhibit similar trends.

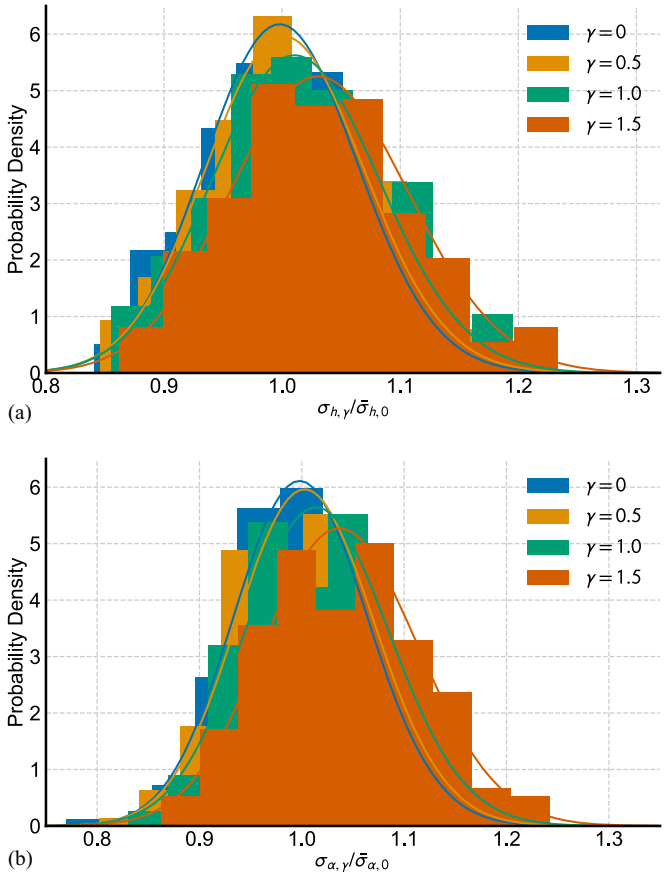

Fig. 17. Increasing RMS responses of 1,800 m span bridge induced by non-Gaussian turbulence with larger skewness ($U = 30$ m/s): (a) vertical response; and (b) torsional response.

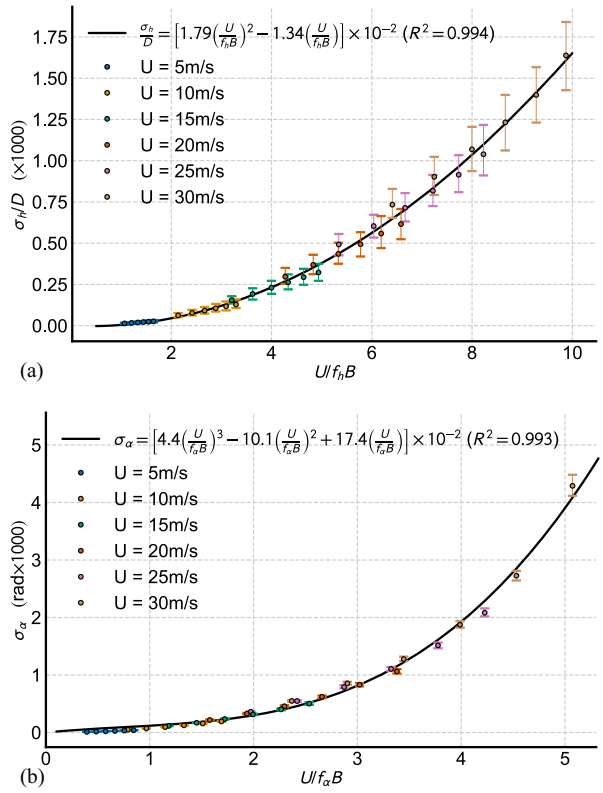

Fig. 18. RMS buffeting responses of bridges with six different spans induced by Gaussian turbulence fitted by a function of normalized wind speeds: (a) vertical response; and (b) torsional response.

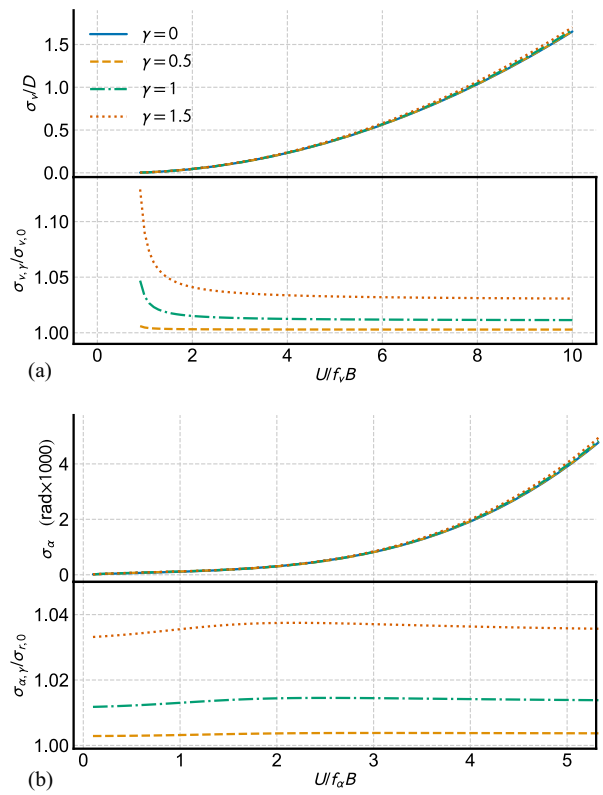

Fig. 19. RMS buffeting responses of bridges with six different spans induced by non-Gaussian turbulence with three different skewness values fitted by a function of normalized wind speeds: (a) vertical response; and (b) torsional response.

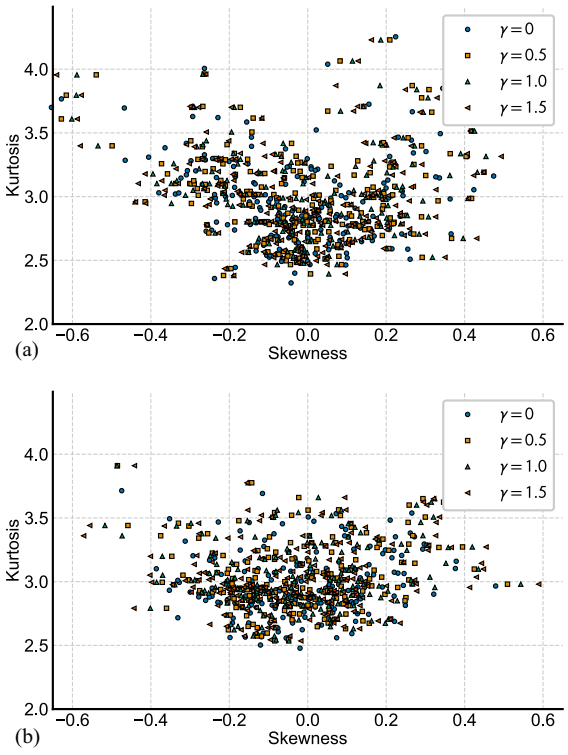

Fig. 20. Correlated skewness and kurtosis distribution comparison of Gaussian and non-Gaussian turbulence-induced bridge buffeting responses with three different skewness values ($U = 30$ m/s, $l = 1$, 200 m): (a) vertical response; and (b) torsional response.

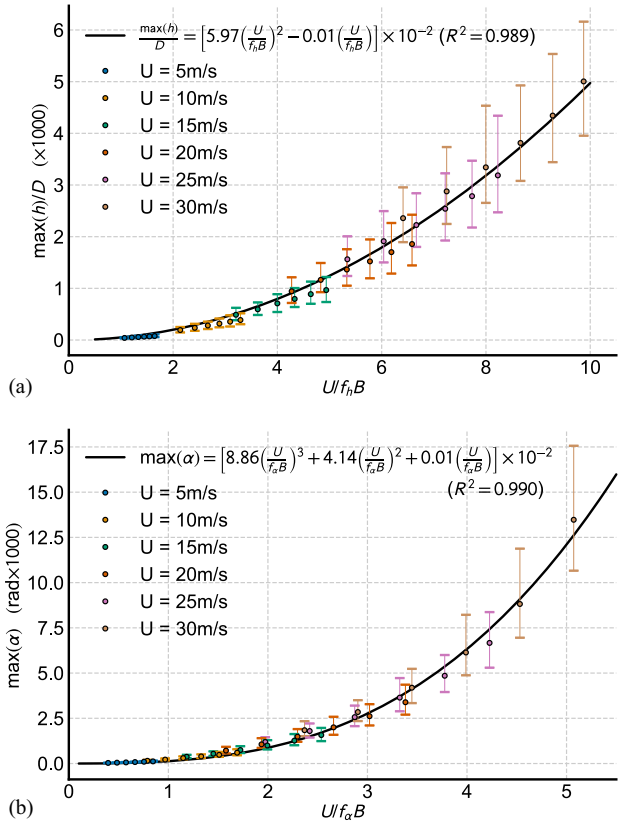

Fig. 21. Peak buffeting response of bridges with six different spans induced by Gaussian turbulence fitted by a function of normalized wind speeds: (a) vertical response; and (b) torsional response.

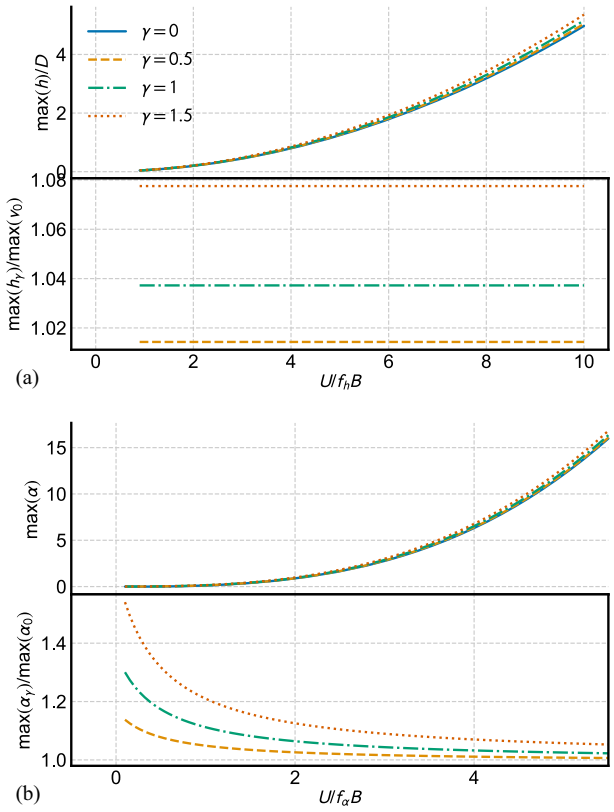

Fig. 22. Peak buffeting response of bridges with six different spans induced by non-Gaussian turbulence with three different skewness values fitted by a function of normalized wind speeds: (a) vertical response; and (b) torsional response.

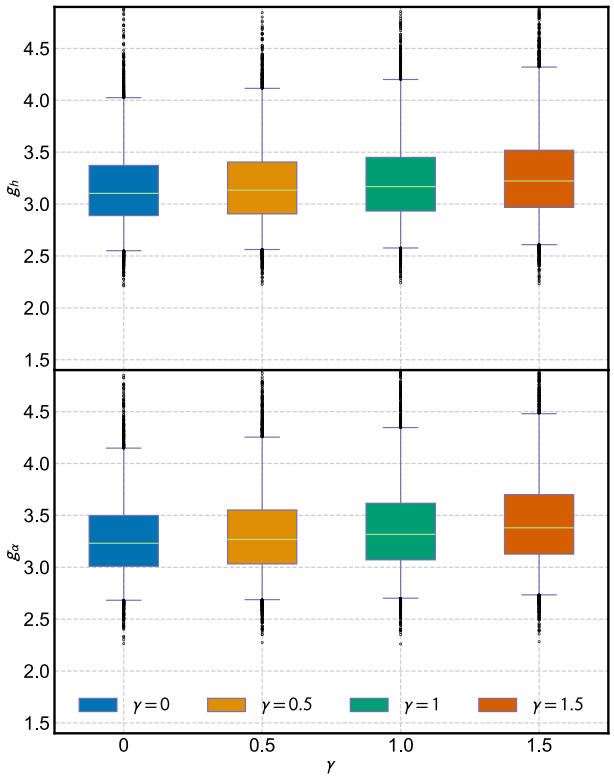

Fig. 23. Box plots of peak factors of Gaussian and non-Gaussian turbulence-induced buffeting responses.

In summary, non-Gaussian turbulence with nonzero skewness normally generates a larger extreme buffeting response. Generally, the larger peak response is because of a greater RMS value rather than peak factors, because turbulence skewness only slightly affects the peak factors.

Conclusions

This paper first discussed the non-Gaussian turbulence characteristics measured from high-frequency typhoon wind records. The results show that the skewness of typhoon wind turbulence can be as high as approximately 1. To perform the time domain analysis of long-span bridges excited by non-Gaussian turbulence, correlated multivariate Gaussian and non-Gaussian turbulence wind fields along the bridge are required. This study utilized the spectral representation method to generate Gaussian turbulence, and the correlation distortion method based on the Hermit function translation process was used to generate non-Gaussian turbulence. Three non-Gaussian cases, with skewness $\gamma = 0.5$, 1.0, 1.5, were selected in this study.

Comparing the bridge buffeting response induced by skewed non-Gaussian turbulence against vibration results caused by Gaussian turbulence, it is concluded that turbulence skewness may increase the range for each periodic vibration. The spectral analysis shows that the response varies with respect to the resonant vibration rather than the background vibration. Finally, a Monte Carlo analysis with 200 samples demonstrated that both RMS and extreme vibration increase along with increase turbulence skewness, but the increasing ratio comparing the baseline Gaussian turbulence-induced vibration declines for higher wind speeds. The peak factors of bridge vibration are slightly affected by turbulence skewness. High-order statistical analysis showed that the bridge buffeting still follows the Gaussian process when the exciting force is non-Gaussian. Therefore, the chi-square distribution can effectively fit the RMS responses from Monte Carlo simulation.

However, it should be noted that the bridge deck aerodynamic force from non-Gaussian turbulence is still assumed to follow the same rule as the Gaussian turbulence, and it requires further experimental verification in the future. In addition to aerodynamic force and response, the wind environment on the bridge deck, which is more sensitive to inflow conditions, is also worth investigation.

Data Availability Statement

All data, models, and code generated or used during the study appear in the published article.

Acknowledgments

The authors gratefully acknowledge the support of National Natural Science Foundation of China (52008314, 52078383) and Shanghai Pujiang Plan (No. 19PJ1409800). Any opinions, findings, and conclusions or recommendations are those of the authors and do not necessarily reflect the views of these agencies.

References

Cai, C., and S. Chen. 2004. "Framework of vehicle–bridge–wind dynamic analysis." *J. Wind Eng. Ind. Aerodyn.* 92 (7-8): 579–607. https://doi.org/10.1016/j.jweia.2004.03.007.

Cao, S., Y. Tamura, N. Kikuchi, M. Saito, I. Nakayama, and Y. Matsuzaki. 2009. "Wind characteristics of a strong typhoon." *J. Wind Eng. Ind. Aerodyn.* 97 (1): 11–21. https://doi.org/10.1016/j.jweia.2008.10.002.

Chen, X., M. Matsumoto, and A. Kareem. 2000a. "Aerodynamic coupling effects on flutter and buffeting of bridges." *J. Eng. Mech.* 126 (1): 17–26. https://doi.org/10.1061/(ASCE)0733-9399(2000)126:1(17).

Chen, X., M. Matsumoto, and A. Kareem. 2000b. "Time domain flutter and buffeting response analysis of bridges." *J. Eng. Mech.* 126 (1): 7–16. https://doi.org/10.1061/(ASCE)0733-9399(2000)126:1(7).

Cui, W., and L. Caracoglia. 2017. "Examination of experimental variability in HFFB testing of a tall building under multi-directional winds." *J. Wind Eng. Ind. Aerodyn.* 171: 34–49. https://doi.org/10.1016/j.jweia.2017.09.001.

Cui, W., and L. Caracoglia. 2018. "A fully-coupled generalized model for multi-directional wind loads on tall buildings: A development of the quasi-steady theory." *J. Fluids Struct.* 78: 52–68. https://doi.org/10.1016/j.jfluidstructs.2017.12.008.

Davenport, A. G. 1961. "A statistical approach to the treatment of wind loading on tall masts and suspension bridges." Ph.D. thesis, Dept. of Civil Engineering, Univ. of Bristol.

Davenport, A. G. 1962. "Buffeting of a suspension bridge by storm winds." *J. Struct. Div.* 88 (3): 233–270. https://doi.org/10.1061/JSDEAG.0000773.

Deodatis, G. 1996. "Simulation of ergodic multivariate stochastic processes." *J. Eng. Mech.* 122 (8): 778–787. https://doi.org/10.1061/(ASCE)0733-9399(1996)122:8(778).

Diana, G., D. Rocchi, T. Argentini, and S. Muggiasca. 2010. "Aerodynamic instability of a bridge deck section model: Linear and nonlinear approach to force modeling." *J. Wind Eng. Ind. Aerodyn.* 98 (6–7): 363–374. https://doi.org/10.1016/j.jweia.2010.01.003.

Djenidi, L., R. A. Antonia, M. K. Talluru, and H. Abe. 2017. "Skewness and flatness factors of the longitudinal velocity derivative in wall-bounded flows." *Phys. Rev. Fluids* 2 (6): 064608. https://doi.org/10.1103/PhysRevFluids.2.064608.

Ge, Y., and L. Zhao. 2014. "Wind-excited stochastic vibration of long-span bridge considering wind field parameters during typhoon landfall." *Wind Struct.* 19 (4): 421–441. https://doi.org/10.12989/was.2014.19.4.421.

Gioffre, M., V. Gusella, and M. Grigoriu. 2000. "Simulation of non-Gaussian field applied to wind pressure fluctuations." *Probab. Eng. Mech.* 15 (4): 339–345. https://doi.org/10.1016/S0266-8920(99)00035-1.

Grigoriu, M. 1984. "Crossings of non-Gaussian translation processes." *J. Eng. Mech.* 110 (4): 610–620. https://doi.org/10.1061/(ASCE)0733-9399(1984)110:4(610).

Grigoriu, M., and S. T. Ariaratnam. 1988. "Response of linear systems to polynomials of Gaussian processes." *J. Appl. Mech.* 55 (4): 905–910. https://doi.org/10.1115/1.3173740.

Gusella, V., and A. Materazzi. 2000. "Non-Gaussian along-wind response analysis in time and frequency domains." *Eng. Struct.* 22 (1): 49–57. https://doi.org/10.1016/S0141-0296(98)00074-1.

Hu, L., Y.-L. Xu, Q. Zhu, A. Guo, and A. Kareem. 2017. "Tropical storm–induced buffeting response of long-span bridges: Enhanced nonstationary buffeting force model." *J. Struct. Eng.* 143 (6): 04017027. https://doi.org/10.1061/(ASCE)ST.1943-541X.0001745.

Hui, Y., B. Li, H. Kawai, and Q. Yang. 2017. "Non-stationary and non-Gaussian characteristics of wind speeds." *Wind Struct.* 24 (1): 59–78. https://doi.org/10.12989/was.2017.24.1.059.

Isyumov, N. 2012. "Alan G. Davenport's mark on wind engineering." *J. Wind Eng. Ind. Aerodyn.* 104: 12–24. https://doi.org/10.1016/j.jweia.2012.02.007.

Jain, A., N. P. Jones, and R. H. Scanlan. 1996. "Coupled flutter and buffeting analysis of long-span bridges." *J. Struct. Eng.* 122 (7): 716–725. https://doi.org/10.1061/(ASCE)0733-9445(1996)122:7(716).

Jones, N. P., and R. H. Scanlan. 2001. "Theory and full-bridge modeling of wind response of cable-supported bridges." *J. Bridge Eng.* 6 (6): 365–375. https://doi.org/10.1061/(ASCE)1084-0702(2001)6:6(365).

Kareem, A., and T. Wu. 2013. "Wind-induced effects on bluff bodies in turbulent flows: Nonstationary, non-Gaussian and nonlinear features." *J. Wind Eng. Ind. Aerodyn.* 122: 21–37. https://doi.org/10.1016/j.jweia.2013.06.002.

Kareem, A., and T. Wu. 2016. "Bluff body aerodynamics and aeroelasticity: Nonstationary, non-Gaussian and nonlinear features." In *Advances in fluid-structure interaction*, edited by M. Braza, A. Bottaro and M. Thompson, 3–14. Cham, Switzerland: Springer.

Karmakar, D., S. Ray-Chaudhuri, and M. Shinozuka. 2012. "Conditional simulation of non-Gaussian wind velocity profiles: Application to buffeting response of vincent thomas suspension bridge." *Probab. Eng. Mech.* 29: 167–175. https://doi.org/10.1016/j.probengmech.2011.11.005.

Katsuchi, H., N. P. Jones, and R. H. Scanlan. 1999. "Multimode coupled flutter and buffeting analysis of the Akashi-Kaikyo bridge." *J. Struct. Eng.* 125 (1): 60–70. https://doi.org/10.1061/(ASCE)0733-9445(1999)125:1(60).

Ko, J., S. Xue, and Y. Xu. 1998. "Modal analysis of suspension bridge deck units in erection stage." *Eng. Struct.* 20 (12): 1102–1112. https://doi.org/10.1016/S0141-0296(97)00207-1.

Le, T.-H., and L. Caracoglia. 2015. "Reduced-order Wavelet-Galerkin solution for the coupled, nonlinear stochastic response of slender buildings in transient winds." *J. Sound Vib.* 344: 179–208. https://doi.org/10.1016/j.jsv.2015.01.007.

Le, V., and L. Caracoglia. 2019. "Generation and characterization of a non-stationary flow field in a small-scale wind tunnel using a multi-blade flow device." *J. Wind Eng. Ind. Aerodyn.* 186: 1–16. https://doi.org/10.1016/j.jweia.2018.12.017.

Li, L., A. Kareem, Y. Xiao, L. Song, and C. Zhou. 2015. "A comparative study of field measurements of the turbulence characteristics of typhoon and hurricane winds." *J. Wind Eng. Ind. Aerodyn.* 140: 49–66. https://doi.org/10.1016/j.jweia.2014.12.008.

Li, Y., and A. Kareem. 1990. "Arma systems in wind engineering." *Probab. Eng. Mech.* 5 (2): 49–59. https://doi.org/10.1016/S0266-8920(08)80001-X.

Liu, M., L. Peng, G. Huang, Q. Yang, and Y. Jiang. 2020. "Simulation of stationary non-Gaussian multivariate wind pressures using moment-based piecewise hermite polynomial model." *J. Wind Eng. Ind. Aerodyn.* 196: 104041. https://doi.org/10.1016/j.jweia.2019.104041.

Monahan, A. H. 2004. "A simple model for the skewness of global sea surface winds." *J. Atmos. Sci.* 61 (16): 2037–2049. https://doi.org/10.1175/1520-0469(2004)061<2037:ASMFTS>2.0.CO;2.

Piccardo, G., and G. Solari. 1998. "Closed form prediction of 3-D wind-excited response of slender structures." *J. Wind Eng. Ind. Aerodyn.* 74: 697–708. https://doi.org/10.1016/S0167-6105(98)00063-4.

Piccardo, G., and G. Solari. 2000. "3D wind-excited response of slender structures: Closed-form solution." *J. Struct. Eng.* 126 (8): 936–943. https://doi.org/10.1061/(ASCE)0733-9445(2000)126:8(936).

Scanlan, R. 1978a. "The action of flexible bridges under wind, I: Flutter theory." *J. Sound Vib.* 60 (2): 187–199. https://doi.org/10.1016/S0022-460X(78)80028-5.

Scanlan, R. 1978b. "The action of flexible bridges under wind, II: Buffeting theory." *J. Sound Vib.* 60 (2): 201–211. https://doi.org/10.1016/S0022-460X(78)80029-7.

Scanlan, R. H. 1984. "Role of indicial functions in buffeting analysis of bridges." *J. Struct. Eng.* 110 (7): 1433–1446. https://doi.org/10.1061/(ASCE)0733-9445(1984)110:7(1433).

Scanlan, R. H., and N. P. Jones. 1990. "Aeroelastic analysis of cable-stayed bridges." *J. Struct. Eng.* 116 (2): 279–297. https://doi.org/10.1061/(ASCE)0733-9445(1990)116:2(279).

Sears, W. R. 1941. "Some aspects of non-stationary airfoil theory and its practical application." *J. Aeronaut. Sci.* 8 (3): 104–108. https://doi.org/10.2514/8.10655.

Seo, D.-W., and L. Caracoglia. 2012. "Statistical buffeting response of flexible bridges influenced by errors in aeroelastic loading estimation." *J. Wind Eng. Ind. Aerodyn.* 104: 129–140. https://doi.org/10.1016/j.jweia.2012.03.036.

Seo, D.-W., and L. Caracoglia. 2013. "Estimating life-cycle monetary losses due to wind hazards: Fragility analysis of long-span bridges." *Eng. Struct.* 56: 1593–1606. https://doi.org/10.1016/j.engstruct.2013.07.031.

Shinozuka, M. 1974. "Digital simulation of random processes in engineering mechanics with the aid of FFT technique (Fast Fourier Fransformation)." In *Stochastic problems in mechanics*, edited by

S. T. Ariaratnam and H. H. E. Leipholz, 277–286. Waterloo, ON, Canada: University of Waterloo Press.
Simiu, E., and R. H. Scanlan. 1996. *Wind effects on structures: Fundamentals and applications to design*. 3rd ed. Hoboken, NJ: John Wiley & Sons.
Simiu, E., and D. Yeo. 2019. *Wind effects on structures: Modern structural design for wind*. 4th ed. Hoboken, NJ: Wiley–Blackwell.
Tabeling, P., G. Zocchi, F. Belin, J. Maurer, and H. Willaime. 1996. "Probability density functions, skewness, and flatness in large Reynolds number turbulence." *Phys. Rev. E* 53 (2): 1613. https://doi.org/10.1103/PhysRevE.53.1613.
Theodorsen, T. 1935. "General theory of aerodynamic instability and the mechanism of flutter."
Wang, H., T. Wu, T. Tao, A. Li, and A. Kareem. 2016. "Measurements and analysis of non-stationary wind characteristics at Sutong Bridge in Typhoon Damrey." *J. Wind Eng. Ind. Aerodyn.* 151: 100–106. https://doi.org/10.1016/j.jweia.2016.02.001.
Welch, P. 1967. "The use of fast fourier transform for the estimation of power spectra: A method based on time averaging over short, modified periodograms." *IEEE Trans. Audio Electroacoust.* 15 (2): 70–73. https://doi.org/10.1109/TAU.1967.1161901.
Wu, F., G. Huang, and M. Liu. 2020. "Simulation and peak value estimation of non-Gaussian wind pressures based on Johnson transformation model." *J. Eng. Mech.* 146 (1): 04019116. https://doi.org/10.1061/(ASCE)EM.1943-7889.0001697.
Wu, T., and A. Kareem. 2013. "A nonlinear convolution scheme to simulate bridge aerodynamics." *Comput. Struct.* 128: 259–271. https://doi.org/10.1016/j.compstruc.2013.06.004.
Xu, Y., D. Sun, J. Ko, and J. Lin. 1998. "Buffeting analysis of long span bridges: A new algorithm." *Comput. Struct.* 68 (4): 303–313. https://doi.org/10.1016/S0045-7949(98)00072-8.
Xu, Y.-L., and W. Guo. 2003. "Dynamic analysis of coupled road vehicle and cable-stayed bridge systems under turbulent wind." *Eng. Struct.* 25 (4): 473–486. https://doi.org/10.1016/S0141-0296(02)00188-8.
Xu, Y.-L., Z.-X. Tan, L.-D. Zhu, Q. Zhu, and S. Zhan. 2019. "Buffeting-induced stress analysis of long-span twin-box-beck bridges based on POD pressure modes." *J. Wind Eng. Ind. Aerodyn.* 188: 397–409. https://doi.org/10.1016/j.jweia.2019.03.016.
Yang, L., and K. R. Gurley. 2015. "Efficient stationary multivariate non-Gaussian simulation based on a Hermite pdf model." *Probab. Eng. Mech.* 42: 31–41. https://doi.org/10.1016/j.probengmech.2015.09.006.
Yang, Q., X. Chen, and M. Liu. 2019. "Bias and sampling errors in estimation of extremes of non-Gaussian wind pressures by moment-based translation process models." *J. Wind Eng. Ind. Aerodyn.* 186: 214–233. https://doi.org/10.1016/j.jweia.2019.01.006.
Yang, Q., and Y. Tian. 2015. "A model of probability density function of non-Gaussian wind pressure with multiple samples." *J. Wind Eng. Ind. Aerodyn.* 140: 67–78. https://doi.org/10.1016/j.jweia.2014.11.005.
Yang, Y., T. Ma, and Y. Ge. 2015. "Evaluation on bridge dynamic properties and VIV performance based on wind tunnel test and field measurement." *Wind Struct.* 20 (6): 719–737. https://doi.org/10.12989/was.2015.20.6.719.
Zhao, L., W. Cui, and Y. Ge. 2019. "Measurement, modeling and simulation of wind turbulence in typhoon outer region." *J. Wind Eng. Ind. Aerodyn.* 195: 104021. https://doi.org/10.1016/j.jweia.2019.104021.